

Study of $\psi(2S)$ decays to XJ/ψ

M. Ablikim¹, J. Z. Bai¹, Y. Ban¹⁰, J. G. Bian¹, X. Cai¹, J. F. Chang¹, H. F. Chen¹⁶, H. S. Chen¹, H. X. Chen¹, J. C. Chen¹, Jin Chen¹, Jun Chen⁶, M. L. Chen¹, Y. B. Chen¹, S. P. Chi², Y. P. Chu¹, X. Z. Cui¹, H. L. Dai¹, Y. S. Dai¹⁸, Z. Y. Deng¹, L. Y. Dong¹, S. X. Du¹, Z. Z. Du¹, J. Fang¹, S. S. Fang², C. D. Fu¹, H. Y. Fu¹, C. S. Gao¹, Y. N. Gao¹⁴, M. Y. Gong¹, W. X. Gong¹, S. D. Gu¹, Y. N. Guo¹, Y. Q. Guo¹, Z. J. Guo¹⁵, F. A. Harris¹⁵, K. L. He¹, M. He¹¹, X. He¹, Y. K. Heng¹, H. M. Hu¹, T. Hu¹, G. S. Huang^{1†}, L. Huang⁶, X. P. Huang¹, X. B. Ji¹, Q. Y. Jia¹⁰, C. H. Jiang¹, X. S. Jiang¹, D. P. Jin¹, S. Jin¹, Y. Jin¹, Y. F. Lai¹, F. Li¹, G. Li¹, H. B. Li^{1‡}, H. H. Li¹, J. Li¹, J. C. Li¹, Q. J. Li¹, R. B. Li¹, R. Y. Li¹, S. M. Li¹, W. G. Li¹, X. L. Li⁷, X. Q. Li⁹, X. S. Li¹⁴, Y. F. Liang¹³, H. B. Liao⁵, C. X. Liu¹, F. Liu⁵, Fang Liu¹⁶, H. M. Liu¹, J. B. Liu¹, J. P. Liu¹⁷, R. G. Liu¹, Z. A. Liu¹, Z. X. Liu¹, F. Lu¹, G. R. Lu⁴, J. G. Lu¹, C. L. Luo⁸, X. L. Luo¹, F. C. Ma⁷, J. M. Ma¹, L. L. Ma¹¹, Q. M. Ma¹, X. Y. Ma¹, Z. P. Mao¹, X. H. Mo¹, J. Nie¹, Z. D. Nie¹, S. L. Olsen¹⁵, H. P. Peng¹⁶, N. D. Qi¹, C. D. Qian¹², H. Qin⁸, J. F. Qiu¹, Z. Y. Ren¹, G. Rong¹, L. Y. Shan¹, L. Shang¹, D. L. Shen¹, X. Y. Shen¹, H. Y. Sheng¹, F. Shi¹, X. Shi¹⁰, H. S. Sun¹, S. S. Sun¹⁶, Y. Z. Sun¹, Z. J. Sun¹, X. Tang¹, N. Tao¹⁶, Y. R. Tian¹⁴, G. L. Tong¹, G. S. Varner¹⁵, D. Y. Wang¹, J. Z. Wang¹, K. Wang¹⁶, L. Wang¹, L. S. Wang¹, M. Wang¹, P. Wang¹, P. L. Wang¹, S. Z. Wang¹, W. F. Wang¹, Y. F. Wang¹, Zhe Wang¹, Z. Wang¹, Zheng Wang¹, Z. Y. Wang¹, C. L. Wei¹, D. H. Wei³, N. Wu¹, Y. M. Wu¹, X. M. Xia¹, X. X. Xie¹, B. Xin⁷, G. F. Xu¹, H. Xu¹, Y. Xu¹, S. T. Xue¹, M. L. Yan¹⁶, F. Yang⁹, H. X. Yang¹, J. Yang¹⁶, S. D. Yang¹, Y. X. Yang³, M. Ye¹, M. H. Ye², Y. X. Ye¹⁶, L. H. Yi⁶, Z. Y. Yi¹, C. S. Yu¹, G. W. Yu¹, C. Z. Yuan¹, J. M. Yuan¹, Y. Yuan¹, Q. Yue¹, S. L. Zang¹, Yu. Zeng¹, Y. Zeng⁶, B. X. Zhang¹, B. Y. Zhang¹, C. C. Zhang¹, D. H. Zhang¹, H. Y. Zhang¹, J. Zhang¹, J. Y. Zhang¹, J. W. Zhang¹, L. S. Zhang¹, Q. J. Zhang¹, S. Q. Zhang¹, X. M. Zhang¹, X. Y. Zhang¹¹, Y. J. Zhang¹⁰, Y. Y. Zhang¹, Yiyun Zhang¹³, Z. P. Zhang¹⁶, Z. Q. Zhang⁴, D. X. Zhao¹, J. B. Zhao¹, J. W. Zhao¹, M. G. Zhao⁹, P. P. Zhao¹, W. R. Zhao¹, X. J. Zhao¹, Y. B. Zhao¹, Z. G. Zhao^{1*}, H. Q. Zheng¹⁰, J. P. Zheng¹, L. S. Zheng¹, Z. P. Zheng¹, X. C. Zhong¹, B. Q. Zhou¹, G. M. Zhou¹, L. Zhou¹, N. F. Zhou¹, K. J. Zhu¹, Q. M. Zhu¹, Y. C. Zhu¹, Y. S. Zhu¹, Yingchun Zhu¹, Z. A. Zhu¹, B. A. Zhuang¹, B. S. Zou¹.

(BES Collaboration)

¹ Institute of High Energy Physics, Beijing 100039, People's Republic of China

² China Center for Advanced Science and Technology(CCAST), Beijing 100080, People's Republic of China

³ Guangxi Normal University, Guilin 541004, People's Republic of China

⁴ Henan Normal University, Xinxiang 453002, People's Republic of China

⁵ Huazhong Normal University, Wuhan 430079, People's Republic of China

⁶ Hunan University, Changsha 410082, People's Republic of China

⁷ Liaoning University, Shenyang 110036, People's Republic of China

⁸ Nanjing Normal University, Nanjing 210097, People's Republic of China

⁹ Nankai University, Tianjin 300071, People's Republic of China

¹⁰ Peking University, Beijing 100871, People's Republic of China

¹¹ Shandong University, Jinan 250100, People's Republic of China

¹² Shanghai Jiaotong University, Shanghai 200030, People's Republic of China

¹³ Sichuan University, Chengdu 610064, People's Republic of China

¹⁴ Tsinghua University, Beijing 100084, People's Republic of China

¹⁵ University of Hawaii, Honolulu, Hawaii 96822

¹⁶ University of Science and Technology of China, Hefei 230026, People's Republic of China

¹⁷ Wuhan University, Wuhan 430072, People's Republic of China

¹⁸ Zhejiang University, Hangzhou 310028, People's Republic of China

* Visiting professor to University of Michigan, Ann Arbor, MI 48109 USA

† Current address: Purdue University, West Lafayette, Indiana 47907, USA

‡ Current address: University of Wisconsin at Madison, Madison WI 5370, USA.

(Dated: February 7, 2008)

Using $J/\psi \rightarrow \mu^+\mu^-$ decays from a sample of approximately 4×10^6 $\psi(2S)$ events collected with the BESII detector, the branching fractions of $\psi(2S) \rightarrow \eta J/\psi$, $\pi^0\pi^0 J/\psi$, and anything J/ψ normalized to that of $\psi(2S) \rightarrow \pi^+\pi^- J/\psi$ are measured. The results are $B(\psi(2S) \rightarrow \eta J/\psi)/B(\psi(2S) \rightarrow \pi^+\pi^- J/\psi) = 0.098 \pm 0.005 \pm 0.010$, $B(\psi(2S) \rightarrow \pi^0\pi^0 J/\psi)/B(\psi(2S) \rightarrow \pi^+\pi^- J/\psi) = 0.570 \pm 0.009 \pm 0.026$, and $B(\psi(2S) \rightarrow \text{anything } J/\psi)/B(\psi(2S) \rightarrow \pi^+\pi^- J/\psi) = 1.867 \pm 0.026 \pm 0.055$.

I. INTRODUCTION

Transitions of the type $\psi(2S) \rightarrow XJ/\psi$ comprise a large fraction of the total $\psi(2S)$ decay width. They include exclusive decays where $X = \eta$, π^0 , and $\pi\pi$, as well as the cascade processes $\psi(2S) \rightarrow \gamma\chi_{c0/1/2}$, $\chi_{c0/1/2} \rightarrow \gamma J/\psi$. The inclusive branching fraction is measured to be $B(\psi(2S) \rightarrow \text{anything } J/\psi) = (55.7 \pm 2.6)\%$; the contributions from the individual sub-processes are less precisely known [1].

These branching fractions are important in understanding the hadronic decay dynamics of vector charmonia [2, 3], since the inclusive hadronic decay branching fraction is calculated by subtracting them from unity. Present branching fractions may indicate a possible excess of the $\psi(2S)$ hadronic decay rate relative to the "12% rule" prediction from J/ψ decays.

Recently the BES experiment reported new measurements with improved precision for $B(\psi(2S) \rightarrow \pi^0 J/\psi)$, $B(\psi(2S) \rightarrow \eta J/\psi)$, and $B(\psi(2S) \rightarrow \gamma\chi_{c0/1/2})B(\chi_{c0/1/2} \rightarrow \gamma J/\psi)$ using decays $\psi(2S) \rightarrow \gamma\gamma J/\psi$, $J/\psi \rightarrow \ell^+\ell^-$, (where $\ell^+\ell^- = \mu^+\mu^-$ or e^+e^-) [4]. Previous measurements are few and date back to the 1970's and 80's [5–9]. More precise measurements are needed.

In this paper, we report the results of a different technique for measuring branching fractions for the inclusive decay $\psi(2S) \rightarrow \text{anything } J/\psi$, and the exclusive processes for the cases where $X = \eta$ and $X = \pi\pi$. We reconstruct $\mu^+\mu^-$ pairs and determine the number of $\psi(2S) \rightarrow XJ/\psi$ events in our data sample from the $J/\psi \rightarrow \mu^+\mu^-$ peak in the $\mu^+\mu^-$ invariant mass distribution (see Fig. 1). The exclusive branching fractions are determined from fits to the distribution of masses recoiling from the J/ψ with Monte-Carlo determined distributions for each individual channel. We distinguish the $\pi^+\pi^-$ and $\pi^0\pi^0$ contributions from simultaneous fits to event samples with and without accompanying charged particles. To avoid a number of systematic errors, the channels of interest are normalized to the observed number of $\pi^+\pi^- J/\psi$ events; we report ratios of the studied branching fractions to that for $B(\psi(2S) \rightarrow \pi^+\pi^- J/\psi)$. This analysis is based on a sample of approximately 4×10^6 $\psi(2S)$ events obtained with the Beijing Spectrometer detector (BESI) [10] at the Beijing Electron-Positron Collider (BEPC).

II. BESI DETECTOR AND MONTE CARLO SIMULATIONS

The Beijing Spectrometer, BESI, is a conventional cylindrical magnetic detector that is coaxial with the BEPC colliding e^+e^- beams. It is described in detail in Ref. [10]. A four-layer central drift chamber (CDC) surrounding the beam pipe provides trigger information. Radially outside of the CDC, a forty-layer main drift chamber (MDC) provides tracking and energy-loss (dE/dx) information on charged tracks over 85% of the total solid angle. The momentum resolution is $\sigma_p/p = 1.7\%\sqrt{1+p^2}$ (p in GeV/c), and the dE/dx resolution for hadron tracks for this data sample is $\sim 9\%$. An array of 48 scintillation counters surrounding the MDC provides measurements of the time-of-flight (TOF) of charged tracks with a resolution of ~ 450 ps for hadrons. Outside of the TOF system is a 12 radiation length lead-gas barrel shower counter (BSC), operating in self-quenching streamer mode, that measures the positions and energies of electrons and photons over 80% of the total solid angle. The energy resolution is $\sigma_E/E = 22\%/\sqrt{E}$ (E in GeV). Surrounding the BSC is a solenoid magnet that provides a 0.4 Tesla magnetic field in the central tracking region of the detector. Three double layers of proportional chambers instrument the magnet flux return (MUID) and are used to identify muons with momentum greater than 0.5 GeV/c.

Monte Carlo simulations are used to determine efficiencies and the expected recoil mass distributions for the various processes involved, including $\psi(2S) \rightarrow \gamma\chi_{c1/2}$, $\psi(2S) \rightarrow \pi\pi J/\psi$, and $\psi(2S) \rightarrow \eta J/\psi$ with $J/\psi \rightarrow \mu^+\mu^-$, as well as the background processes $e^+e^- \rightarrow \gamma\mu^+\mu^-$, $e^+e^- \rightarrow \psi(2S)$, $\psi(2S) \rightarrow (\gamma)\mu^+\mu^-$, $e^+e^- \rightarrow 2\gamma^* \rightarrow \mu^+\mu^-e^+e^-$ ($\mu^+\mu^-\mu^+\mu^-$). In each decay, angular distributions are generated according to expectations for that process. The agreement between the distributions of $\cos\theta_\mu$ for data and Monte Carlo has been checked in separate analyses and found to be reasonable. Since the default generator for $\psi(2S) \rightarrow \pi\pi J/\psi$, produces S -wave dipion states, while BES has measured a small but non-negligible amount of D -wave in the dipion system [11], Monte Carlo events are weighted to give the correct angular and m_X distributions.

III. EVENT SELECTION

Selected events are required to have more than one and less than six charged tracks.

A. Muon Selection

Events must have two identified muon tracks with zero net charge. The μ tracks must satisfy:

1. $0.5 < p_\mu < 2.5$ GeV/c. Here p_μ is the three-momentum of the candidate muon track in the lab.
2. $p_{\mu^+} > 1.3$ or $p_{\mu^-} > 1.3$ GeV/c or $(p_{\mu^+} + p_{\mu^-}) > 2.4$ GeV/c. This requirement selects events consistent with J/ψ decay, while rejecting background.
3. $|\cos \theta_\mu| < 0.60$. Here θ_μ is the laboratory polar angle of the muon. This requirement ensures that muons are contained in the MUID system.
4. $\cos \theta_{\mu^+\mu^-} < -0.85$. This is the cosine of the angle between the two leptons in the lab. The leptons from this decay are almost back to back.
5. Both tracks must have $N^{hit} > 1$, where N^{hit} is the number of MUID layers with matched hits and ranges from 0 to 3.
6. $|t_{TOF}(\mu^+) - t_{TOF}(\mu^-)| < 4$ ns. Here t_{TOF} is the time measured by the TOF counters. This requirement removes cosmic ray background.

B. Selection of J/ψ events

For $J/\psi \rightarrow \mu^+\mu^-$ candidates, the two tracks must satisfy a one constraint kinematic fit to the J/ψ mass. Shown in Fig. 1 is the invariant mass distribution of the two muons, $m_{\mu\mu}$, for J/ψ candidates. A clear peak at the J/ψ mass is evident above background. The distribution of χ^2 values from the one-constraint kinematic fits to the $J/\psi \rightarrow \mu^+\mu^-$ hypothesis is shown in Fig. 2. The mass recoiling against the J/ψ candidates, m_X is determined from energy and momentum conservation.

C. Extra track (π) selection

In order to distinguish $\psi(2S) \rightarrow \pi^+\pi^- J/\psi$ and $\psi(2S) \rightarrow \pi^0\pi^0 J/\psi$ events, separate m_X histograms are made for events with no additional charged tracks, those with any number of additional charged tracks, and those with two or more additional charged tracks. The first histogram and one of the other histograms are fitted simultaneously [12]. To reduce background and improve the quality of the track momentum measurements, events used for this part of the analysis are required to have a kinematic fit $\chi^2 < 7$.

Additional charged tracks can originate from $\psi(2S) \rightarrow \pi^+\pi^- J/\psi$ and $\psi(2S) \rightarrow \eta J/\psi$, $\eta \rightarrow \pi^+\pi^-\gamma/\pi^0$ decays, and also from gamma conversions and delta rays. Selection criteria are applied to the additional tracks to enhance the selection of low energy pion tracks, such as those coming from the process $\psi(2S) \rightarrow \pi^+\pi^- J/\psi$, and reject gamma conversions and delta rays.

1. Tracks must have a good helix fit with:
2. $p_\pi < 0.5$ GeV/c, where p_π is the pion momentum;
3. $|\cos \theta_\pi| < 0.8$, where θ_π is the polar angle of the π in the laboratory system;
4. $p_{xy_\pi} > 0.08$ GeV/c, where p_{xy_π} is the momentum of the pion transverse to the beam direction (this removes tracks that circle in the MDC);
5. $|\chi_\pi^{dE/dx}| < 3.0$. $\chi_\pi^{dE/dx} = \frac{(dE/dx)_{meas} - (dE/dx)_{exp}}{\sigma}$, where $(dE/dx)_{meas}$ and $(dE/dx)_{exp}$ are the measured and expected dE/dx energy losses for pions, respectively, and σ is the experimental dE/dx resolution.
6. For events with more than one additional tracks, $\cos \theta_{\pi\pi} < 0.9$, where $\theta_{\pi\pi}$ is the laboratory angle between them. This last requirement reduces contamination from misidentified e^+e^- pairs from γ conversions.

The m_X histograms for events with and without additional charged tracks, selected according to the above requirements, are shown in Figs. 3 and 4.

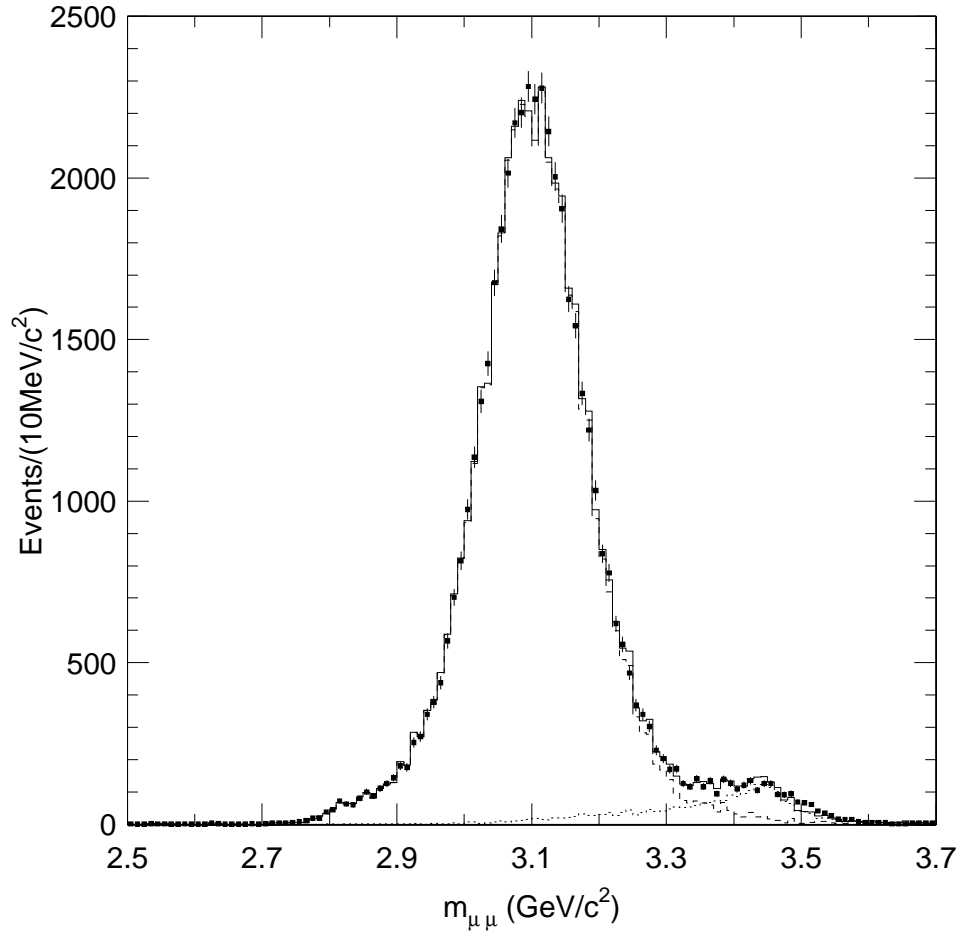


FIG. 1: Distribution of dimuon invariant mass, $m_{\mu\mu}$, for events that pass the $J/\psi \rightarrow \mu^+\mu^-$ kinematic fit. Dots with error bars are data. Also shown is the fit (solid histogram) to the distribution with signal (long dashed histogram) and background (short dashed histogram) shapes.

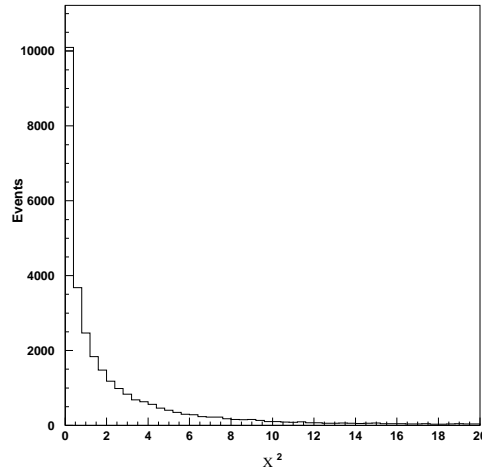


FIG. 2: Distribution of χ^2 (data) for events satisfying a one-constraint kinematic fit to $J/\psi \rightarrow \mu^+\mu^-$.

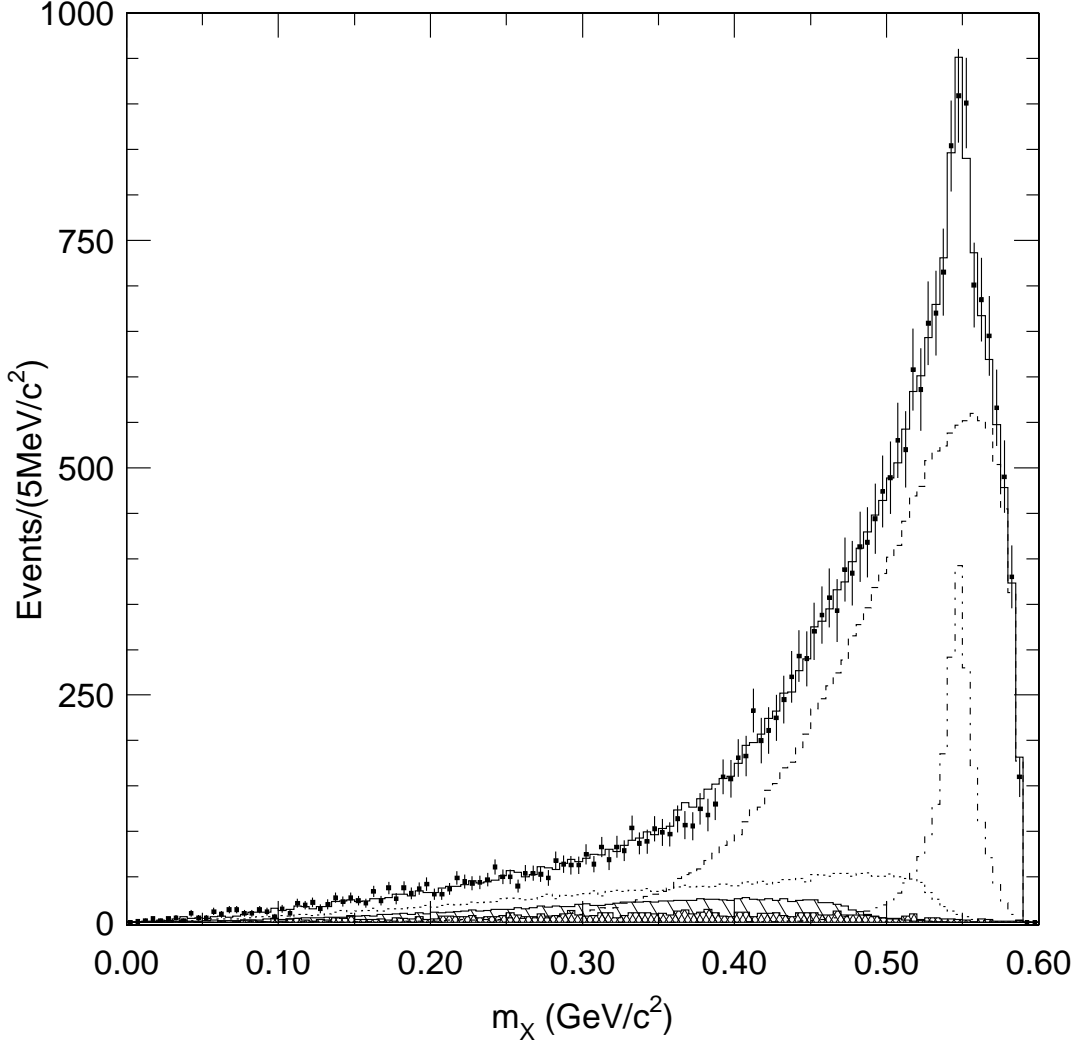


FIG. 3: Fit of the m_X distribution events with no additional charged tracks. Shown are the data (points with error bars), the component histograms, and the final fit. For the components, the large, long-dash histogram is $\psi(2S) \rightarrow \pi\pi J/\psi$, the narrow, dash-dot histogram is $\psi(2S) \rightarrow \eta J/\psi$, the broad, short-dashed histogram is $\psi(2S) \rightarrow \gamma\chi_{c1}$, the broad, hatched histogram is $\psi(2S) \rightarrow \gamma\chi_{c2}$, and the lowest cross-hatched histogram is the combined $e^+e^- \rightarrow \gamma\mu^+\mu^-$ and $e^+e^- \rightarrow \psi(2S), \psi(2S) \rightarrow (\gamma)\mu^+\mu^-$ background. The final fit is the solid histogram.

IV. BACKGROUND STUDIES

The backgrounds from $e^+e^- \rightarrow \gamma\mu^+\mu^-$ and $e^+e^- \rightarrow \psi(2S), \psi(2S) \rightarrow (\gamma)\mu^+\mu^-$ in the $m_{\mu\mu}$ and m_X distributions are measured using data. We begin by considering what backgrounds are expected.

A. Expected backgrounds

Possible background processes are $e^+e^- \rightarrow \gamma\mu^+\mu^-$, $e^+e^- \rightarrow \psi(2S), \psi(2S) \rightarrow (\gamma)\mu^+\mu^-$, and $e^+e^- \rightarrow 2\gamma^* \rightarrow \mu^+\mu^-e^+e^- (\mu^+\mu^-\mu^+\mu^-)$. The number of background events expected from the simulation of $e^+e^- \rightarrow 2\gamma^* \rightarrow \mu^+\mu^-e^+e^-$ in the $m_{\mu\mu}$ distribution is four events, which is negligible. The background in the m_X distribution with no extra charged tracks is even smaller, and the calculated backgrounds for $e^+e^- \rightarrow \mu^+\mu^-\mu^+\mu^-$ are determined to be smaller still. The numbers of two photon background events are found to be entirely negligible, and this process is ignored further.

The Monte Carlo (MC)-determined level of $e^+e^- \rightarrow \gamma\mu^+\mu^-$ background in the $m_{\mu\mu}$ [13] distribution and the m_X distribution with no additional tracks [14] are 556 ± 20 , and 192 ± 10 events, respectively. For $e^+e^- \rightarrow$

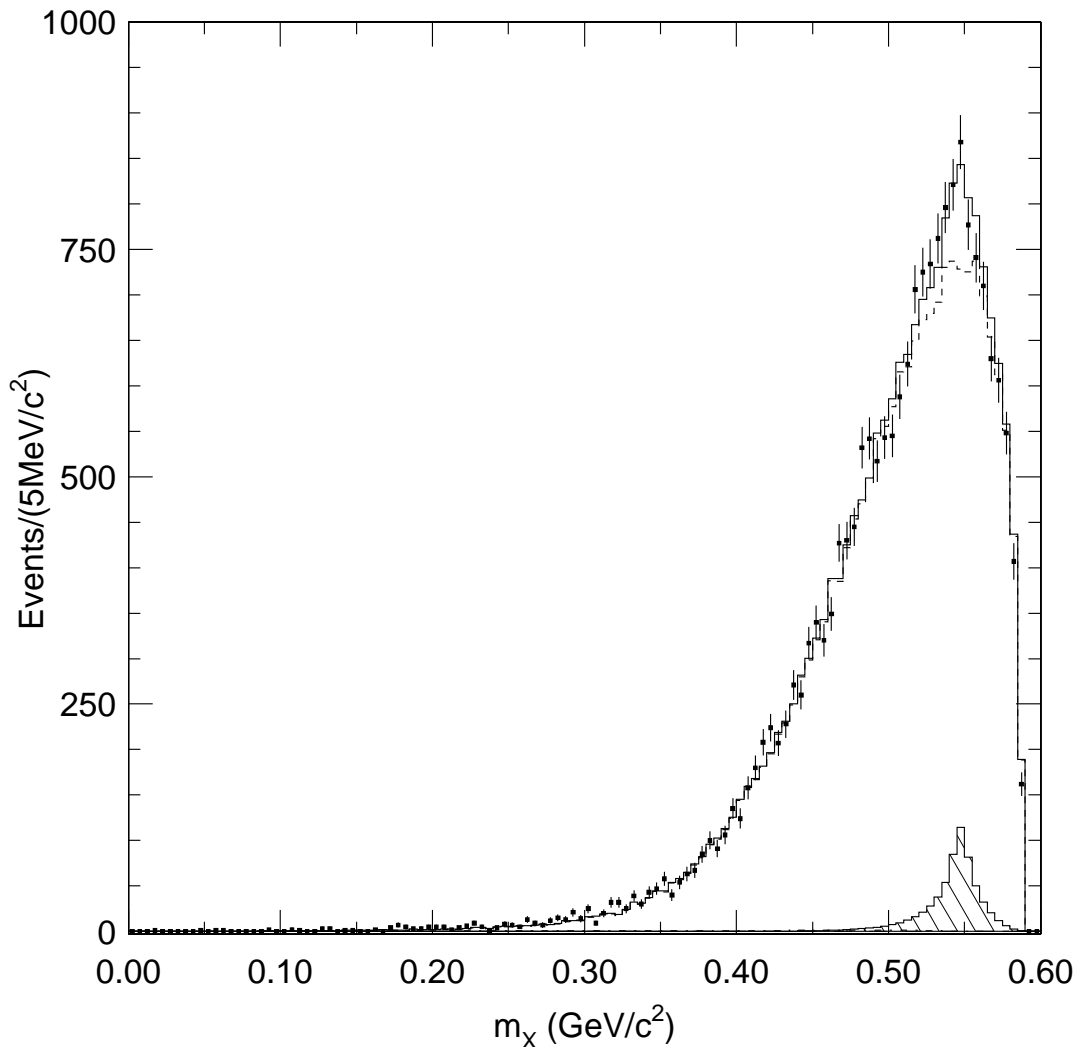


FIG. 4: Fit of the m_X distribution for events with any number of additional charged tracks. Shown are the data (points with error bars), the component histograms, and the final fit (solid histogram). The dashed histogram is $\psi(2S) \rightarrow \pi^+\pi^-J/\psi$, and the hatched histogram is $\psi(2S) \rightarrow \eta J/\psi$. There is very little evidence for $\chi_{c1/2}$. This distribution is composed predominantly of $\psi(2S) \rightarrow \pi^+\pi^-J/\psi$.

$\psi(2S), \psi(2S) \rightarrow (\gamma)\mu^+\mu^-$, the expected background in these distributions are 430 ± 67 and 137 ± 22 events, and the total backgrounds are 986 ± 70 and 329 ± 24 events, respectively. The result obtained from fitting the background level in the $m_{\mu\mu}$ distribution (Fig. 1) is 1307 ± 56 events which is larger than the MC-determined background level. The background shapes and the numbers of background events estimated for the two processes are similar, so the histograms are combined in the fitting of the two distributions.

B. Inclusive Background

1. Determination of $e^+e^- \rightarrow \gamma\mu^+\mu^-$ background from the $\cos\theta_{J/\psi}$ distribution.

The photon from $e^+e^- \rightarrow \gamma\mu^+\mu^-$ is typically emitted along the beam direction, producing a dimuon system which is along the beam in the opposite direction. The cosine of the angle of the J/ψ in the lab, $\cos\theta_{J/\psi}$, shows a strong peaking near ± 1 for simulated $e^+e^- \rightarrow \gamma\mu^+\mu^-$ events, as shown in Fig. 5b. Some peaking near ± 1 is also found in the data, as shown for the case with no χ^2 requirement in Fig. 5a. By fitting the $\cos\theta_{J/\psi}$ distribution for data with the $e^+e^- \rightarrow \gamma\mu^+\mu^-$ Monte Carlo distribution plus a distribution to represent the non-peaked events, a total

of 839 ± 98 background events is obtained. This can be compared with the predicted $e^+e^- \rightarrow \gamma\mu^+\mu^-$ background estimate of 556 ± 20 events in the $m_{\mu\mu}$ distribution. The difference is 283 ± 100 .

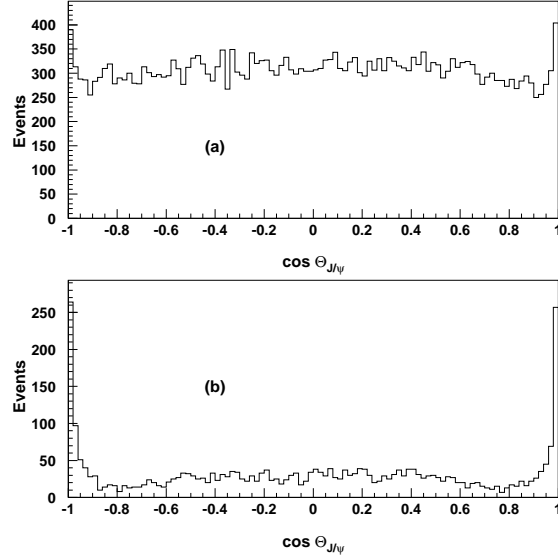


FIG. 5: The distribution of the cosine of the angle of the J/ψ in the lab, $\cos\theta_{J/\psi}$, for a.) data and b.) simulated $e^+e^- \rightarrow \gamma\mu^+\mu^-$ events. The peaks at $|\cos\theta_{J/\psi}| = 1$ indicate some $e^+e^- \rightarrow \gamma\mu^+\mu^-$ background in the data. No χ^2 requirement is made for these plots but $m_{\mu\mu} < 3.4$ GeV/c².

An additional source of background, not included in the $e^+e^- \rightarrow \gamma\mu^+\mu^-$ simulation, is due to “radiative return” to the J/ψ peak, $e^+e^- \rightarrow \gamma J/\psi$, $J/\psi \rightarrow \mu^+\mu^-$. This background is similar to the signal in the $m_{\mu^+\mu^-}$ distribution and would not be part of the background determined from the fit to the $m_{\mu^+\mu^-}$ distribution. However, it would be included in the background determined from the $\cos\theta_{J/\psi}$ distribution. The difference between the background determined from the $\cos\theta_{J/\psi}$ distribution and the predicted $e^+e^- \rightarrow \gamma\mu^+\mu^-$ is taken as a measure of the radiative return.

2. Total background from the $\Delta\phi$ distribution

Since the μ^+ and μ^- from $e^+e^- \rightarrow \gamma\mu^+\mu^-$, $e^+e^- \rightarrow \psi(2S)$, $\psi(2S) \rightarrow (\gamma)\mu^+\mu^-$, and the “radiative return” background processes are coplanar, it is possible to determine their level from the $\Delta\phi$ distributions of the data, where $\Delta\phi$ is the difference between the ϕ angles of the μ^+ and the μ^- ($\pm 180^\circ$). Fig. 6 shows the Monte Carlo and data distributions for $\Delta\phi$. The $e^+e^- \rightarrow \gamma\mu^+\mu^-$ and $e^+e^- \rightarrow \psi(2S)$, $\psi(2S) \rightarrow (\gamma)\mu^+\mu^-$ distributions show a large peak at 0° , which is not seen in other simulations. A similar peak is seen in the data. The $\Delta\phi$ distribution from data is fitted using Monte Carlo distributions, including the combined $e^+e^- \rightarrow \gamma\mu^+\mu^-$ and $e^+e^- \rightarrow \psi(2S)$, $\psi(2S) \rightarrow (\gamma)\mu^+\mu^-$ $\Delta\phi$ distribution plus a broad distribution to represent the other processes. The fit determines 1476 ± 150 background events in the $m_{\mu\mu}$ distribution. The result is summarized in Table I, along with estimates obtained by adding the “radiative return” determined using the $\cos\theta_{J/\psi}$ distribution to the predicted and measured background from the $m_{\mu\mu}$ distribution. The agreement between the various methods to estimate the background is reasonable.

C. Exclusive Background

The predicted background from $e^+e^- \rightarrow \gamma\mu^+\mu^-$ and $e^+e^- \rightarrow \psi(2S)$, $\psi(2S) \rightarrow (\gamma)\mu^+\mu^-$ in the m_X distribution is smaller than that in the $\mu^+\mu^-$ distribution. However “radiative return” which is not included in the Monte Carlo generator is not expected to be reduced by the χ^2 requirement that is made in going from the $m_{\mu^+\mu^-}$ distribution to the m_X distribution.

As was done above, the $\cos\theta_{J/\psi}$ distribution (but now with a χ^2 requirement) can be used to determine the amount of $e^+e^- \rightarrow \gamma\mu^+\mu^-$ background in the m_X distribution. Using a similar calculation, the amount of background is determined to be 413 ± 75 events. The measured background is larger than the predicted background, and the

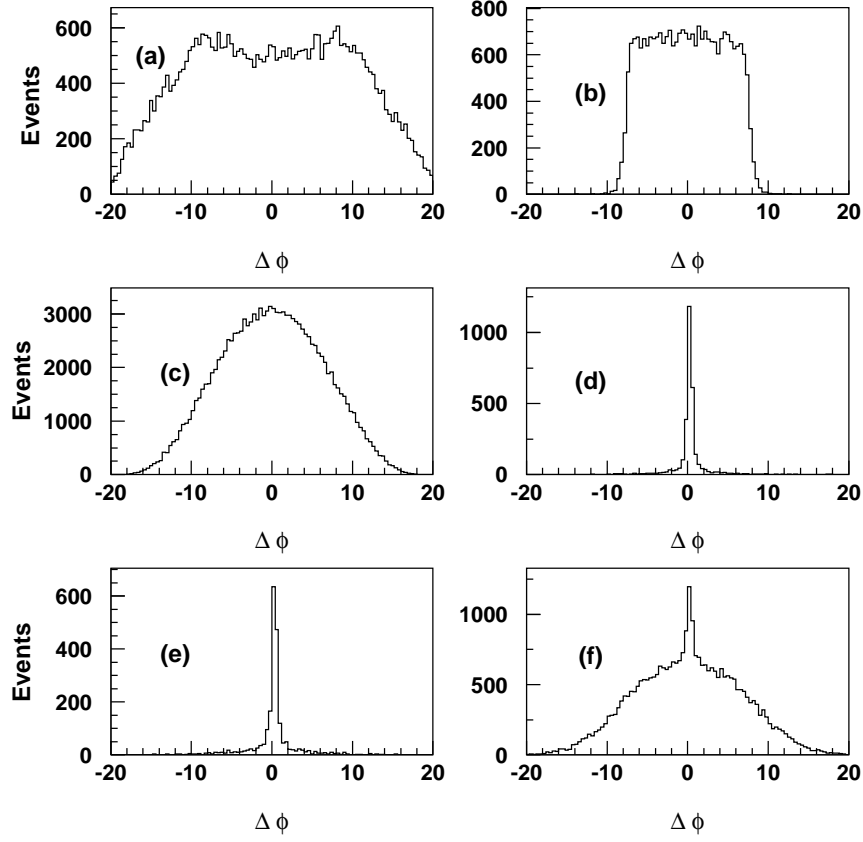


FIG. 6: $\Delta\phi$ distribution for a.) $\gamma\chi_{c1}$, b.) $\eta J/\psi$, c.) $\pi^+\pi^- J/\psi$, d.) $e^+e^- \rightarrow \gamma\mu^+\mu^-$, e.) $e^+e^- \rightarrow \psi(2S), \psi(2S) \rightarrow \gamma\mu^+\mu^-$, and f.) data. No χ^2 requirement is made for these plots.

TABLE I: Backgrounds in the $m_{\mu\mu}$ and m_X distributions from $e^+e^- \rightarrow \gamma\mu^+\mu^-$ and $e^+e^- \rightarrow \psi(2S), \psi(2S) \rightarrow (\gamma)\mu^+\mu^-$ events that pass the selection criteria. Predicted results are from Monte Carlo simulations which do not include radiative return. The $m_{\mu\mu}$ is determined above by fitting background in the $m_{\mu\mu}$ distribution. Results are given with the radiative return determined from the difference between the background determined from the $\cos\theta_{J/\psi}$ distribution and the predicted $e^+e^- \rightarrow \gamma\mu^+\mu^-$ background added to the predicted and $m_{\mu\mu}$ results. These may be compared to the determinations obtained fitting the $\Delta\phi$ distributions, which do contain radiative return.

Distribution	Predicted + Meas. Rad. Ret.	$m_{\mu\mu}$ + Meas. Rad. Ret.	$\Delta\phi$ Dist.
$m_{\mu^+\mu^-}$	1269 ± 122	1590 ± 140	1476 ± 150
m_X	550 ± 80	—	636 ± 161

difference (221 ± 76) is taken as a measurement of the “radiative return”. Note that the two determinations of “radiative return” are consistent as expected.

The $\Delta\phi$ distributions with a χ^2 requirement may be used, as above, to determine the total background in the m_X distribution including “radiative return”. The result is 636 ± 161 events. The amount of background when fitting the m_X distributions will be constrained to this amount. Table I compares the estimates and final backgrounds determined from $\Delta\phi$ distributions for both the $m_{\mu\mu}$ and m_X backgrounds. The agreement between the various determinations for each distribution is reasonable, and the total backgrounds are quite small.

V. FITTING THE MASS DISTRIBUTIONS

A. Inclusive channel

To determine the number of inclusive events, the $m_{\mu^+\mu^-}$ distribution is fit with signal and background shapes. The signal shape is obtained from real data using the $m_{\mu^+\mu^-}$ distributions from $\psi(2S) \rightarrow \text{anything } J/\psi$ (data) events with additional charged tracks. These events are primarily due to $\pi^+\pi^- J/\psi$. For the background shape, the $m_{\mu^+\mu^-}$ distribution obtained by combining the distributions for Monte Carlo $e^+e^- \rightarrow \gamma\mu^+\mu^-$ and $e^+e^- \rightarrow \psi(2S)$, $\psi(2S) \rightarrow (\gamma)\mu^+\mu^-$ events is used. Figure 1 shows the fit to the $m_{\mu^+\mu^-}$ distribution. The background distribution differs somewhat from the data in the high mass region. Because of this, the fit and background determinations everywhere in this analysis are restricted to masses below $3.4 \text{ GeV}/c^2$. The background in the $m_{\mu^+\mu^-}$ distribution (Fig. 1) below $3.4 \text{ GeV}/c^2$ is determined to be 1307 ± 56 events. The number of events in the signal peak is 44498.

B. Exclusive decays

To determine the number of exclusive decays and separate $\psi(2S) \rightarrow \pi^0\pi^0 J/\psi$ and $\psi(2S) \rightarrow \pi^+\pi^- J/\psi$ events, m_X histograms for events with and without additional charged tracks, shown in Figs. 3 and 4, are fit simultaneously. There are 20818 and 19846 events in the two distributions. Contributions from the χ_{c0} are expected to be very small [15] and are not included in the fit. The influence of $\psi(2S) \rightarrow \pi^0 J/\psi$ is also small, indeed there is no indication of such a component in Fig. 3, and this channel is also not included. The m_X distributions for χ_{c1} , χ_{c2} , and the combined background distribution are broad and rather similar in shape, as can be seen in Fig. 3. Since these are difficult to distinguish, the χ_{c2} to χ_{c1} ratio is constrained using calculated efficiencies and the PDG world average branching fractions for the two processes. In addition, the amount of background is constrained as discussed above.

In Fig. 4, it is seen that the χ_{c1} , χ_{c2} , and η contributions are small. When fitting, the ratios of these components to those in Fig. 3 are also constrained using Monte Carlo determined ratios. Since the amount of background is predicted to be very small in this distribution, it is not included in the fit. The numbers of fitted events obtained from the simultaneous fits to the m_X distributions of Figs. 3 and 4 and corresponding efficiencies are shown in Table II.

As an indication as to how well the Monte Carlo distributions fit the signal, Figs. 7 and 8 show the data with all but one shape subtracted, normalized using the fit results, and compared with the Monte Carlo distribution.

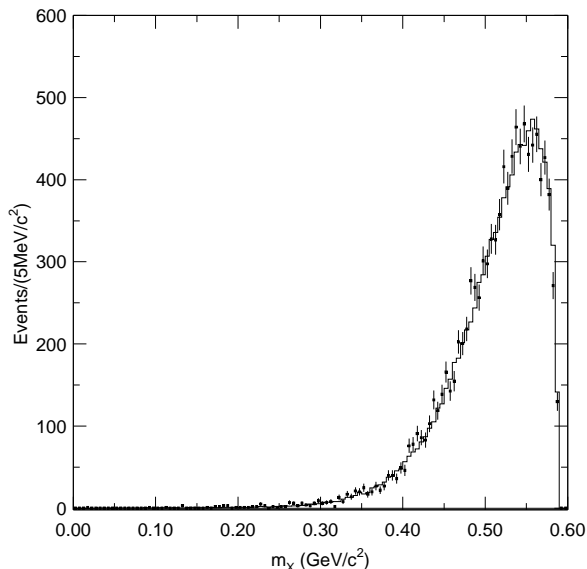


FIG. 7: Data with two or more additional charged tracks with all Monte Carlo distributions, normalized by the fit result, subtracted except for $\pi\pi$ (dots with error bars), fit with $\psi(2S) \rightarrow \pi\pi J/\psi$ Monte Carlo (solid histogram) plus a polynomial.

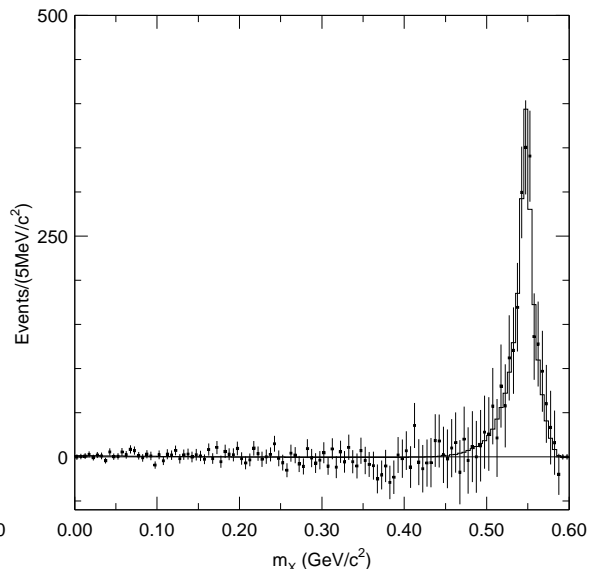


FIG. 8: Data with no additional charged tracks with all Monte Carlo distributions, normalized by the fit result, subtracted except for $\eta J/\psi$ (dots with error bars), fit with $\psi(2S) \rightarrow \eta J/\psi$ Monte Carlo (solid histogram) plus a polynomial.

TABLE II: Fit results and efficiencies for inclusive and exclusive decays. The exclusive results are for fitting the distributions shown in Figs. 3 and 4 simultaneously. The numbers of events, n , and the efficiencies (eff) for the exclusive cases are the results for the histogram in Fig. 3. The zero error on the number of χ_{c2} events is because of the χ_{c2}/χ_{c1} constraint.

CASE	n	δn	eff
Anything ($m_{\mu\mu}$)	44498	232	0.3488
$\pi^+\pi^-$ and $\pi^0\pi^0$	13952	186	0.150
η	2121	117	0.3597
χ_{c1}	2793	62	0.3678
χ_{c2}	1326	0	0.3661

C. Determination of branching ratios

Ratios of branching fractions, normalizing to the number of $\psi(2S) \rightarrow \pi^+\pi^- J/\psi$ events, i.e. $\frac{B(\psi(2S) \rightarrow X J/\psi)}{B(\psi(2S) \rightarrow \pi^+\pi^- J/\psi)}$ are calculated. The advantage of normalizing in this way is that many of the muon selection systematic errors largely cancel, as well as the systematic error due to the χ^2 requirement.

First the correction factor for $\pi^0\pi^0$ events in the $\pi\pi$ m_X distribution with additional charged tracks (f_1) due to gamma conversions and delta rays is determined:

$$f_1 = \frac{0.305\epsilon_1(\pi^+\pi^-)}{0.305\epsilon_1(\pi^+\pi^-) + 0.182\epsilon_1(\pi^0\pi^0)},$$

where $\epsilon_1(\pi^+\pi^-)$ and $\epsilon_1(\pi^0\pi^0)$ are the efficiencies for additional charged tracks for $\pi^+\pi^-$ and $\pi^0\pi^0$ events, respectively, and 0.305 and 0.182 are the PDG branching fractions for $\psi(2S) \rightarrow \pi^+\pi^- J/\psi$ and $\psi(2S) \rightarrow \pi^0\pi^0 J/\psi$, respectively [1].

$$N_1(\pi^+\pi^-) = f_1 N_1(\pi\pi),$$

where $N_1(\pi\pi)$ is the number of $\pi\pi$ events with additional charged tracks. Since $\epsilon_1(\pi^0\pi^0)$ is small, f_1 is near 1.0: $f_1 = 0.967$.

For $X = \eta$ or $X = \chi_c$,

$$\frac{B(\psi(2S) \rightarrow X J/\psi)}{B(\psi(2S) \rightarrow \pi^+\pi^- J/\psi)} = \frac{\epsilon_{\text{ratio1}} \epsilon_1(\pi^+\pi^-) N_0(X)}{\epsilon_0(X) f_1 N_1(\pi\pi)},$$

where ϵ_{ratio1} is ratio of the track efficiencies for detecting one π track for data and Monte Carlo data, $N_0(X)$ is the number of X events in the histogram with no additional tracks, and $\epsilon_0(X)$ is the efficiency for X 's in the same sample. For the $\pi^0\pi^0$ case:

$$\frac{B(\psi(2S) \rightarrow \pi^0\pi^0 J/\psi)}{B(\psi(2S) \rightarrow \pi^+\pi^- J/\psi)} = \frac{\epsilon_{\text{ratio1}} \epsilon_1(\pi^+\pi^-) N_0(\pi\pi)}{\epsilon_0(\pi^0\pi^0) f_1 N_1(\pi\pi)} - \frac{\epsilon_0(\pi^+\pi^-)}{\epsilon_0(\pi^0\pi^0)},$$

where $N_0(\pi\pi)$ is the number of events in the $\pi\pi$ peak in the histogram with no additional tracks.

For the $X \rightarrow$ anything case, the $m_{\mu\mu}$ distribution that is fitted to obtain the number of $\psi(2S) \rightarrow$ anything J/ψ events, $N(\text{anything } J/\psi)$, has no χ^2 requirement. Therefore a correction must be made for the effect of this requirement since a χ^2 requirement was made on the $\psi(2S) \rightarrow \pi^+\pi^- J/\psi$ distribution:

$$\frac{B(\psi(2S) \rightarrow \text{anything } J/\psi)}{B(\psi(2S) \rightarrow \pi^+\pi^- J/\psi)} = \left(\frac{\epsilon_{\text{ratio1}} \epsilon_1(\pi^+\pi^-)}{\epsilon(\text{anything } J/\psi)} \right) \left(\frac{\epsilon_{\chi^2 \text{ cut}} N(\text{anything } J/\psi)|_{\text{no } \chi^2 \text{ cut}}}{N_1(\pi^+\pi^- J/\psi)} \right)$$

The efficiencies in the first fraction on the right of the equal sign are determined from Monte Carlo and have a χ^2 requirement. The term $\epsilon(\text{anything } J/\psi)$ is the efficiency for the combination of processes in $\psi(2S) \rightarrow$ anything J/ψ . The term $\epsilon_{\chi^2 \text{ cut}}$ is the efficiency of the χ^2 requirement and is determined using data from the ratio of events with additional tracks with and without the χ^2 requirement. By requiring an extra charged track, a clean sample of events with which to determine this ratio is selected.

The m_X analysis is done using the distributions shown in Figs. 3 and 4. It may also be done using the distribution for events with more than one additional charged tracks rather than the one with any number of additional charged tracks. Each has its advantages. The first case has a higher efficiency and should have a smaller percentage error on the efficiency. The second one should have less background from delta rays and gamma conversions. Our final results are determined from the averages of the results for these two cases and are summarized in Table IV.

VI. SYSTEMATIC ERRORS

Systematic errors are summarized in Table III. Some of them are determined by varying selection requirements. Other contributions are determined by turning off the weighting used for $\psi(2S) \rightarrow \pi\pi J/\psi$ events, smearing the simulated m_X by $\sigma = 3$ MeV to test the effect of changing the mass resolution, and removing constraints. The amount of smearing of m_X was determined by comparing the width of a Gaussian fit to the η peak for data in Fig. 8 with a Gaussian fit to the corresponding Monte Carlo distribution. The data width is possibly 2 MeV wider (added in quadrature) than the Monte Carlo width.

As shown in Fig. 5b, the $\cos\theta_{J/\psi}$ distribution, where $\theta_{J/\psi}$ is the angle of the J/ψ in the lab, shows some peaking near ± 1.0 , which is indicative of background from the radiative process. To check whether this background is being handled correctly, the effect of an additional requirement on this angle ($|\cos\theta_{J/\psi}| < 0.9$) is determined and included in the systematic errors. The background estimate in the m_X distribution has also been increased by 30 % to determine the systematic error due to the uncertainty in the amount of background.

In the study done in Ref. [16], the gamma conversion rate in data versus Monte Carlo data was compared, and it was found that the rate was lower in data, (4.0 ± 0.15) %, than in Monte Carlo data, 4.5 %. The effect of this difference has been studied using two different methods. In the first, the efficiencies for extra charged tracks in neutral decays is changed by 4.0/4.5. In the second approach, a much higher track momentum requirement ($p_{xy\pi} > 0.15$ GeV/c) is made since gamma conversions are predicted by the Monte Carlo simulation to be more important at lower momentum.

This analysis has been done for two cases. The first uses the distribution with any number of additional charged tracks, while the second uses the distribution with more than one additional charged tracks. For our final results, the averages of the two sets of values are used, and one half the difference between them is included in the systematic errors. Also included is an uncertainty of 2 % for the uncertainty in ϵ_{ratio1} .

TABLE III: Systematic error summary. The total error uses 1/2 the difference of the fitting results for the greater than zero and the greater than one extra charged track cases in quadrature with all the other errors. Here $B(00) = B(\psi(2S) \rightarrow \pi^0\pi^0 J/\psi)$, $B(+-) = B(\psi(2S) \rightarrow \pi^+\pi^- J/\psi)$, $B(\eta) = B(\psi(2S) \rightarrow \eta J/\psi)$, $B(\chi_{c1}) = B(\psi(2S) \rightarrow \gamma\chi_{c1})$, $B(\chi_{c2}) = B(\psi(2S) \rightarrow \gamma\chi_{c2})$, and $B(\text{anything}) = B(\psi(2S) \rightarrow \text{anything } J/\psi)$.

Variation	$\frac{B(00)}{B(+-)}$ (%)	$\frac{B(\eta)}{B(+-)}$ (%)	$\frac{B(\chi_{c1})}{B(+-)}$ (%)	$\frac{B(\chi_{c2})}{B(+-)}$ (%)	$\frac{B(\text{anything})}{B(+-)}$ (%)
$1.3 \times m_X$ background	0.26	0.67	5.44	5.44	—
$p_{xy\pi} > 0.08 \rightarrow > 0.15$ GeV/c	0.88	0.34	0.74	0.51	0.22
lower γ conversion	1.11	1.01	0.74	1.04	—
$ \cos\theta_\pi < 0.8 \rightarrow 0.75$	0.17	0.67	0.25	0.0	0.26
$ \chi_{dE/dx} < 3.0 \rightarrow < 5.0$	1.93	0.67	0.99	1.04	0.73
$\chi^2 < 7 \rightarrow < 10$	0.12	2.35	0.25	0.0	0.03
$ \cos\theta_\mu < 0.6 \rightarrow 0.65$	0.29	0.0	0.74	1.04	0.19
$y_{\text{mid}} > 1 \rightarrow > 0$	0.47	3.69	0.99	1.04	0.09
$ t_{\text{TOF}}(\mu^+) - t_{\text{TOF}}(\mu^-) < 4 \rightarrow < 5$	0.29	0.0	0.25	0.0	0.14
unweight $m_{\pi\pi}$	1.70	5.70	3.47	3.62	0.12
smear mass (3 MeV)	0.70	4.36	0.74	0.51	0.42
remove η constraint	0.18	0.34	0.0	0.0	0.17
remove χ_{c2} constraint	1.70	2.35	29.0	46.1	0.45
$ \cos\theta_{J/\psi} < 0.9$	0.29	3.36	2.23	2.59	0.59
ϵ_{ratio1}	2.0	2.0	2.0	2.0	2.0
$> 0 \rightarrow > 1$ extra tracks	4.17	3.05	3.17	2.76	3.48
$m_{\mu^+\mu^-}$ background $\rightarrow e^+e^- \rightarrow \gamma\mu^+\mu^-$ only					0.14
Total	4.58	9.82	29.9	46.8	2.92

Also indicated in Table III are the total systematic errors. They are reasonably small except for $\psi(2S) \rightarrow \gamma\chi_{c1}$ and $\psi(2S) \rightarrow \gamma\chi_{c2}$. The branching ratios are very different when the χ_{c2} constraint is removed.

VII. FINAL RESULTS

The final branching fraction ratios and branching fractions are shown in Table IV, along with the PDG results, including their experimental averages and global fit results. For $B(\psi(2S) \rightarrow \pi^0\pi^0 J/\psi)/B(\psi(2S) \rightarrow \pi^+\pi^- J/\psi)$, the

PDG does not use the previous experimental results and gives no average value. For the other four branching fraction ratios, only one measurement exists for each, and Table IV lists the single measurements quoted by the PDG. Our results for $B(\text{anything } J/\psi)/B(\psi(2S) \rightarrow \pi^+\pi^- J/\psi)$ and $B(\eta J/\psi)/B(\psi(2S) \rightarrow \pi^+\pi^- J/\psi)$ have smaller errors than the previous results. As a check, the sum of the exclusive branching fraction ratios in the top of Table IV add to 1.854 ± 0.094 , which is in good agreement with the inclusive branching fraction ratio (1.867 ± 0.026), where the errors are the fit errors only.

To determine the branching fractions, the ratios are multiplied by the PDG2002 value for $B(\psi(2S) \rightarrow \pi^+\pi^- J/\psi) = (30.5 \pm 1.6) \%$. The agreement for both the ratios of branching fractions and the calculated branching fractions using the PDG result for $\psi(2S) \rightarrow B(\pi^+\pi^- J/\psi)$ with the PDG fit results is good. The χ_c results are high compared to the PDG by about one sigma.

TABLE IV: Final branching ratios and branching fractions. PDG02-exp results are single measurements or averages of measurements, while PDG02-fit are results of their global fit to many experimental measurements. For the value marked by *, the PDG gives the reciprocal. The BES results in the second half of the table are calculated using the PDG value of $B_{\pi\pi} = B(\psi(2S) \rightarrow \pi^+\pi^- J/\psi) = (30.5 \pm 1.6)\%$.

Case	This result	PDG02-exp	PDG02-fit
$B(\text{anything } J/\psi)/B_{\pi\pi}$	$1.867 \pm 0.026 \pm 0.055$	2.016 ± 0.150 [17]	$1.828 \pm 0.036^*$
$B(\pi^0\pi^0 J/\psi)/B_{\pi\pi}$	$0.570 \pm 0.009 \pm 0.026$	-	0.60 ± 0.06
$B(\eta J/\psi)/B_{\pi\pi}$	$0.098 \pm 0.005 \pm 0.010$	0.091 ± 0.021 [8]	0.103 ± 0.010
$B(\gamma\chi_{c1})B(\chi_{c1} \rightarrow \gamma J/\psi)/B_{\pi\pi}$	$0.126 \pm 0.003 \pm 0.038$	0.085 ± 0.021 [8]	0.087 ± 0.007
$B(\gamma\chi_{c2})B(\chi_{c2} \rightarrow \gamma J/\psi)/B_{\pi\pi}$	$0.060 \pm 0.000 \pm 0.028$	0.039 ± 0.012 [8]	0.042 ± 0.004
$B(\text{anything } J/\psi) (\%)$	$56.9 \pm 0.8 \pm 3.4$	55 ± 7	55.7 ± 2.6
$B(\pi^0\pi^0 J/\psi) (\%)$	$17.4 \pm 0.3 \pm 1.2$	-	18.2 ± 1.2
$B(\eta J/\psi) (\%)$	$3.00 \pm 0.16 \pm 0.33$	2.9 ± 0.5	3.13 ± 0.21
$B(\gamma\chi_{c1})B(\chi_{c1} \rightarrow \gamma J/\psi) (\%)$	$3.9 \pm 0.1 \pm 1.2$	2.66 ± 0.16	2.66 ± 0.15
$B(\gamma\chi_{c2})B(\chi_{c2} \rightarrow \gamma J/\psi) (\%)$	$1.84 \pm 0.01 \pm 0.86$	1.20 ± 0.13	1.27 ± 0.08

VIII. SUMMARY

In this analysis, the $m_{\mu^+\mu^-}$ distribution for candidate $J/\psi \rightarrow \mu^+\mu^-$ events is fit to determine $B(\psi(2S) \rightarrow XJ/\psi, X \rightarrow \text{anything})$. Energy - momentum conservation is used to determine the recoil mass, m_X , and the m_X distribution is fit with Monte Carlo determined distributions to determine the number of exclusive decays. All processes are normalized to $\psi(2S) \rightarrow \pi^+\pi^- J/\psi$ to reduce systematic errors. Ratios of the branching fractions of $\psi(2S) \rightarrow \eta J/\psi$, $\pi^0\pi^0 J/\psi$, and anything J/ψ to that of $\psi(2S) \rightarrow \pi^+\pi^- J/\psi$ are measured to be $0.098 \pm 0.005 \pm 0.010$, $0.570 \pm 0.009 \pm 0.026$, and $1.867 \pm 0.026 \pm 0.055$, respectively.

Acknowledgments

The BES collaboration thanks the staff of BEPC for their hard efforts. This work is supported in part by the National Natural Science Foundation of China under contracts Nos. 19991480,10225524,10225525, the Chinese Academy of Sciences under contract No. KJ 95T-03, the 100 Talents Program of CAS under Contract Nos. U-11, U-24, U-25, and the Knowledge Innovation Project of CAS under Contract Nos. U-602, U-34(IHEP); by the National Natural Science Foundation of China under Contract No.10175060(USTC),and No.10225522(Tsinghua University); and by the Department of Energy under Contract No.DE-FG03-94ER40833 (U Hawaii).

-
- [1] K. Hagiwara *et al.*, Phys. Rev. **D66**, 010001 (2002).
 - [2] M. Suzuki, Phys. Rev. **D63**, 054021 (2001).
 - [3] Y. F. Gu and X. H. Li, Phys. Rev. **D63**, 114019 (2001).
 - [4] J. Z. Bai *et al.*, BES Collaboration, submitted to Phys. Rev. **D**, hep-ex/0403023.
 - [5] G. S. Abrams *et al.*, Phys. Rev. Lett. **34**, 1181 (1975);
J. S. Whitaker *et al.*, Phys. Rev. Lett. **37**, 1596 (1976);
W. M. Tanenbaum *et al.*, Phys. Rev. Lett. **36**, 402 (1976).

- [6] C. J. Biddick *et al.* , Phys. Rev. Lett. **38**, 1324 (1977);
W. Bartel *et al.* , Phys. Lett. **B79**, 492 (1978).
- [7] R. Brandelik *et al.* , Nucl .Phys. **B160**, 426 (1979);
R. Brandelik *et al.* , Z. Phys. **C1**, 233 (1979).
- [8] T. Himel *et al.* , Phys. Rev. Lett. **44**, 920 (1980).
- [9] M. J. Oreglia *et al.* , Phys. Rev. Lett. **45**, 959 (1980);
M. J. Oreglia *et al.* , Phys. Rev. **D25**, 2259 (1982);
J. Gaiser *et al.* , Phys. Rev. **D34**, 711 (1986).
- [10] J.Z. Bai *et al.*, (BES Collab.), Nucl. Inst. Meth. **A344**, 319 (1994).
- [11] J. Z. Bai *et al.* , BES Collaboration, Phys. Rev. **D62**, 32002 (2000).
- [12] The fitting of the $m_{\mu\mu}$ and m_X distributions is done using Mn_fit, www-zeus.physik.uni-bonn.de/~brock/mn_fit.html.
- [13] For the $m_{\mu\mu}$ distribution, no χ^2 requirement is made but $m_{\mu\mu} < 3.4 \text{ GeV}/c^2$ is used.
- [14] Here $\chi^2 < 7.0$ is also required.
- [15] From [1], $B(\psi(2S) \rightarrow \gamma\chi_{c0})B(\chi_{c0} \rightarrow \gamma J/\psi)$: $B(\psi(2S) \rightarrow \gamma\chi_{c1})B(\chi_{c1} \rightarrow \gamma J/\psi)$: $B(\psi(2S) \rightarrow \gamma\chi_{c2})B(\chi_{c2} \rightarrow \gamma J/\psi) = 0.026 : 1 : 0.477$
- [16] J.Z. Bai *et al.* , BES Collaboration, Phys. Rev. **D67**, 052002 (2003).
- [17] T. A. Armstrong *et al.* , Phys. Rev. **D55**, 1153 (1997).